# Characterization and Optoelectronic Effects of Iridium-Doped ZnO Thin Films for Heterojunction Applications

**Seval AKSOY PEHLIVANOGLU\*1** [ID] **, Ozgur POLAT2** [ID]

1Sinop Üniversitesi, Fen Edebiyat Fakültesi, Fizik Bölümü, 57000, Sinop, Türkiye
2Tallinn Avrupa Okulu, Tehnika 18, 10149, Tallinn, Estonya

**Abstract:** In this investigation, the sol-gel spin coating technique was utilized to fabricate ZnO and ZnO films doped with Iridium (Ir) onto p-Si substrates. The objective was to analyze their optical and morphological characteristics and assess their potential for heterojunction applications. Morphological inspection and optical evaluation were carried out by Atomic Force Microscopy (AFM) and Ultraviolet-visible (UV-VIS) studies, respectively. With the incorporation of Ir, the optical band gap of ZnO films reduced from 3.21 eV to 3.08 eV. Analysis of AFM images revealed that Ir substitution led to a reduction in the roughness of the surface of the fabricated films. The optoelectrical features of the heterojunction structures were examined under varying illumination levels and in dark conditions. Upon evaluating the optoelectrical characteristics of the produced diodes, it was observed that the ideality factor ($n$) and the barrier height ($\Phi_B$) declined, while series resistance ($R_s$) increased with the introduction of Ir. These findings emphasize that the inclusion of Ir into the ZnO structure has a discernible impact on optical parameters.

# Heteroeklem Uygulamaları için İridyum Katkılı ZnO İnce Filmlerin Karakterizasyonu ve Optoelektronik Etkileri

**Özet:** Bu çalışmada, İridyum (Ir) katkılı ZnO ve ZnO filmleri, sol-jel spin kaplama tekniği kullanılarak p-Si alttaşlar üzerine kaplanmıştır. Amaç, optik ve morfolojik özelliklerini analiz etmek ve heteroeklem uygulamaları için potansiyellerini değerlendirmekti. Morfolojik inceleme ve optik değerlendirme sırasıyla Atomik Kuvvet Mikroskobu (AFM) ve Ultraviyole-görünür (UV-VIS) çalışmaları ile gerçekleştirilmiştir. Ir'nin katkılanmasıyla, ZnO filmlerin optik bant aralığı 3,21 eV'den 3,08 eV'ye düşürüldü. AFM görüntülerinin analizi, Ir ikamesinin üretilen filmlerin yüzey pürüzlülüğünde bir azalmaya yol açtığını ortaya çıkardı. Heteroeklem yapılarının optoelektriksel özellikleri, değişen aydınlatma şiddetleri altında ve karanlık koşullarda incelenmiştir. Üretilen diyotların optoelektrik özellikleri değerlendirildiğinde idealite faktörü (n) ve bariyer yüksekliğinin (ΦB) düştüğü, Ir'nin devreye girmesiyle seri direncin (Rs) arttığı gözlenmiştir. Bu bulgular, Ir'nin ZnO yapısına dahil edilmesinin optik parametreler üzerinde fark edilebilir bir etkiye sahip olduğunu vurgulamaktadır.

## 1. Introduction

For years, there has been extensive attention in the utilization of third-generation wide-bandgap (WBG) semiconductors like GaN, SiC, and ZnO due to their efficient applicability in optoelectronic devices that operate at shorter wavelengths. Among these materials, GaN takes the first place in the field of commercial use. The most important reason for this is that it has an ultra-WBG (~ 6.2 eV). While undoped GaN has a band gap of about 3.4 eV, AlGaN obtained when doped with Al can have a band gap of 6.2 eV. The

difficulties encountered due to the difficulty of obtaining p-type conductivity with high Al doping have enabled the use of ZnO semiconductor material, which has many similarities, instead of GaN in new-generation device applications. In addition to the mentioned similarities, ZnO also has many advantages over GaN. [1]. For example, ZnO demonstrates characteristics such as reduced growth temperature requirements, decreased expenses, a heightened resistance to radiation, and a more substantial exciton binding energy. In addition to these advantages, ZnO has features such as a large gap (3.37 eV), high excitement energy (60 meV), exhibiting piezoelectric material behavior, being biocompatible, and synthesizing as nanomaterial by many methods. These properties are the kind of properties that will cause ZnO to be included in many studies in the future [2]. Variation of band gap of these materials is a critical parameter that determines the commercial viability of [1]. This attribute holds significance across various application domains, particularly in cases where photon absorption or emission is involved, such as in solar cells, photodetectors, solid-state light emitters, and laser systems. The adjustability of the band gap is crucial for enabling optoelectronic devices to function effectively across various wavelengths, allowing for their development and precise control. Band gap tuneability is also a defining feature in the design of heterojunction structures. Considering the importance of optical band gaps for device design, materials with easily controllable band gaps take a step forward in scientific studies. ZnO is just such a material. Responding to the doping process with a band gap change, ZnO has been highly preferred by researchers. When the literature is searched, it is seen that B, Ni, Sb, Zr, Ir, Co, Cu, Mn, Sn, Al, Cd, Fe, and Mg are used as dopants [3-17]. When the studies are examined, it has been reported that some of these dopants increase (B, Ni, Sb, Zr) the band gap value, while some decrease it (Ir, Co, Cu, Mn, Sn, Al, Cd,), while others both increase and decrease it (Fe, Mg) according to the amount of dopant. Typically, in theory, a band gap represents the distinction between the valence band, which holds electrons, and the conduction band, as commonly comprehended. Fundamentally, the band gap represents the least amount of energy needed for an electron to engage in conduction. For this reason, it is a very effective parameter on conductivity [18] A few studies using Ir, one of the dopants mentioned above, are found in the literature. The first of these studies was made by M. Zubkins et al. [7]. The researchers utilized the DC reactive magnetron co-sputtering technique to fabricate thin films of both undoped and ZnO:Ir under room temperature conditions. They then examined how the structural, optical, and electrical characteristics of these thin films varied based on the dopant used. They documented that the optical band gap remained constant across different iridium concentrations. They indicated that the shift in conduction type occurred from being n-type to p-type

when the iridium concentration reached values between 12.4% and 16.4%. Another study was carried out by N. Babajani and S. Jamshidi [8]. The authors synthesized undoped and ZnO:Ir nanoparticles by sonochemical method and explored the optical, morphological, and photocatalytic properties of nanoparticles depending on the amount of Ir dopant. While they found the band gap of the undoped ZnO nanoparticle to be 3.25 eV, they stated that the band gap value decreased to 2.72 eV with the increasing amount of doped (15%Ir-ZnO). Finally, M. Dhanalakshmi et al. [9] synthesized undoped and ZnO:Ir nanocomposites by a one-pot hydrothermal method. They examined how the dopant concentration influenced the structural, morphological, optical, and photocatalytic characteristics of the nanocomposites. They presented that the band gap, which was 3.19 eV, decreased to 2.94 eV with the increasing Ir dopant. When the relevant literature is reviewed, there is an urgent need for studies that can inspire research in this area with a perspective on the future use of ZnO:Ir nanofilm on issues that have not yet been studied and need to be clarified. The present research presents a study based on bandgap engineering and the development of heterojunctions, inspired by several previous studies on Ir doping [7-9,19,20]. This study tries to present the applicability of Ir-doped ZnO nanofilms in heterojunction devices, which has not been encountered in the literature so far. Valence state and Pauling electronegativity are two important parameters that change optical properties, for instance, optical band gap and conductivity of Ir [19,20]. Since Zn and Ir displacements with Pauling electronegativity of 1.65 and 2.20, respectively, are estimated in the current study, anticipated outcomes involve alterations in the optical and electrical attributes of ZnO due to the introduction of iridium. In this ongoing research, thin films of iridium-doped ZnO (6%) were produced on p-Si substrates using the sol-gel spin coating technique. The optical band gap of the films was determined using the specular reflection spectrum. Atomic force microscopy studies were carried out to analyze the surface morphology of the films. Heterojunctions of n-ZnO:Ir/p-Si were manufactured, and the electrical behaviors of the acquired diodes were studied, contingent on the degree of Ir doping.

## 2. Materıals and Methods

### 2.1. Deposition of films and fabrication of Ir:ZnO/p-Si photodiodes

Thin films of ZnO, both without doping and with iridium (Ir) doping, were deposited onto p-Si substrates using the sol-gel spin coating method. The initial substance employed was zinc acetate dihydrate ($Zn(CH_3COO)_2.H_2O$), commonly referred to as ZnAc, and as the dopant source, anhydrous Iridium (III) chloride ($IrCl_3$) was utilized. To create the ZnAc

solution, 2-methoxyethanol ($C_3H_8O_2$) was used as the solvent, with monoethanolamine ($C_2H_7NO$, MEA) serving as a stabilizing agent. The ratio of MEA to ZnAc was maintained at 1:1, and the solution concentration was set at 0.5 M. The Ir/Zn mole ratios were 0% and 6%. Acetic acid was introduced into the solution, which was then dripped onto a p-Si substrate spinning at 3000 rpm for 30 seconds via a spin coater. The films that were applied underwent a drying procedure within a furnace at 300°C for a duration of 10 minutes. This process of coating and drying was repeated two times. Following this, the films were subjected to annealing in an air environment at 500°C for a duration of 1 hour, carried out using a tube furnace. After completing the process of depositing the film, aluminum (Al) electrodes with excellent electrical conduction properties and a thickness of 150 nm were applied to the film using thermal evaporation. This was accomplished by using a shadow mask for precise placement. For the back contact, a silver paste was utilized. The resulting diodes were denoted as ZIRO0 for the n-ZnO/p-Si heterojunction and ZIRO6 for the n-ZnO:Ir 6%/p-Si heterojunction diodes. The schematic representation of the diode structure can be found in Figure 1.
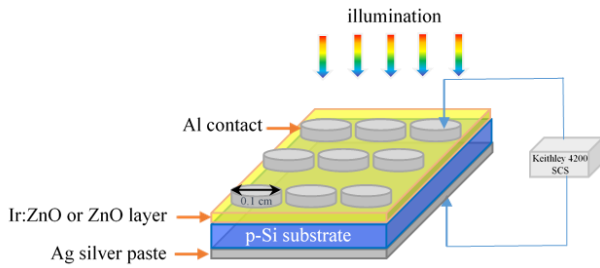


**Figure 1**. Schematic illustration of heterojunction photodiodes

## 2.2. Characterization of films

To conduct photo-electrical evaluations on the films, the process of aluminum evaporation was executed utilizing a vacuum thermal evaporation system named Vaksis PVD (Handy-MT/101T). Modifications in the surface structure of the films were investigated through the utilization of Atomic Force Microscopy (AFM) in both its two-dimensional and three-dimensional modes. Optical properties have been analyzed using a spectrophotometer (Shimadzu 2450 UV). KEITHLEY 4200 SCS/CVU has been utilized to analyze the current-voltage (I-V) behavior of the photodiodes. Measurements were conducted under different levels of illumination using a solar simulator (Asahi-HAL320) equipped with a 1.5AM filter.

## 3. Results

Figure 2 illustrates the spectra of diffuse reflectance percentages for the examined films. Notably, the reflectance of Ir-doped ZnO thin film displays an elevation. This augmentation in diffuse reflectance percentage in ZnO due to Ir doping can be attributed to i) Defects and Trapping Centers: The introduction of Ir into the ZnO structure could potentially introduce defects or centers for trapping. These entities might emerge within the ZnO crystal lattice. As a result, they can function as sites that scatter incident light, leading to an amplified scattering effect and subsequently causing an increase in diffuse reflectance. ii) Surface Morphology: Ir doping holds the capacity to impact the surface attributes of the ZnO film. This influence on surface characteristics can manifest in smoother surfaces, which are discussed below. Such smoother surfaces are adept at enhancing the scattering of light, which ultimately contributes to a higher level of diffuse reflectance.
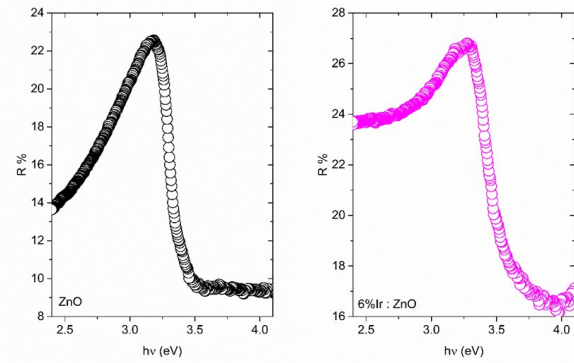


**Figure 2.** Spectral measurements of diffuse reflectance for both the undoped and iridium-doped ZnO thin films.

The determination of band gap values, denoted as $E_g$, is accomplished through the utilization of the Kubelka-Munk function. This approach involves the use of diffuse reflectance (R) spectrum data. The Kubelka-Munk function is employed with the following equation to calculate the $E_g$ value [21]:

$$\left(\frac{F(R)hn}{t}\right)^2 = B(hn - E_g) \tag{1}$$

In this formula, F(R) represents the Kubelka-Munk function, while $t$ signifies thickness. The determination of $E_g$ values involved identifying the point on the linear segment of the graph in Figure 3 where it intersects the energy axis. The calculated $E_g$ values extracted from the Kubelka-Munk relation are 3.21 eV for ZIRO0 and 3.08 eV for ZIRO6. This analysis

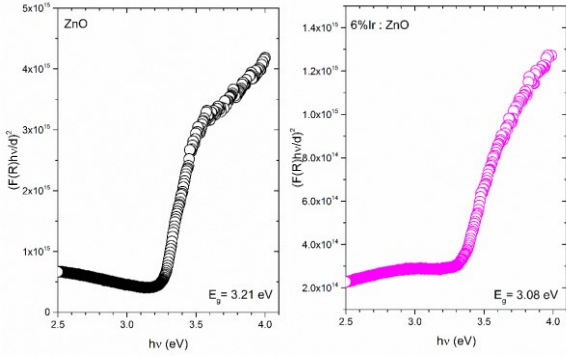indicates a reduction in the $E_g$ value upon introducing the Ir dopant.



**Figure 3.** The optical energy gaps of thin films made from ZnO and ZnO with iridium substitution.

Figure 4 presents both 2D and 3D AFM visuals illustrating the topographical alterations and surface roughness variations in ZIRO0 and ZIRO6 thin films. These images demonstrate the impact of Ir doping on surface characteristics. The surface roughness measurements for the thin films reveal values of 65.12 nm for undoped ZnO and 7.41 nm for ZnO doped with 6% Ir. It has been demonstrated that surface roughness holds an inverse relationship with the films' surface energy [22,23]. Hence, the decrease in surface roughness observed in the Ir-doped film could be associated with a raise in surface energy, promoting the development of smoother surfaces within the studied films.

For a comprehensive exploration of the band diagrams of the deposited films, it is possible to compute the potentials at the conduction edge ($E_{CB}$) and valence edge ($E_{VB}$) using the equations provided below.

$$E_{VB} = \chi - E_e + \frac{1}{2}E_g \qquad (2)$$

$$E_{CB} = E_{VB} - E_g \qquad (3)$$

$$E_0 = -(\chi - E_{CB}) \qquad (4)$$

In this context, the symbols $E_g$, $\chi$, $E_e$ and $E_0$ represent the optically derived band gap value, the absolute electronegativity value of ZnO (approximately 4.35 eV), the energy of a free electron at the hydrogen level (around 4.5 eV), and the vacuum level, respectively. The band position diagram computed for the films is depicted in Figure 5.
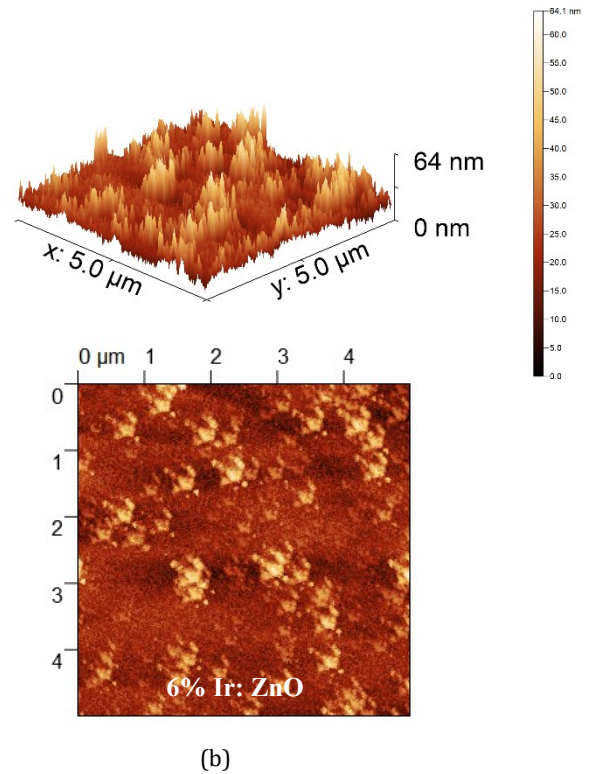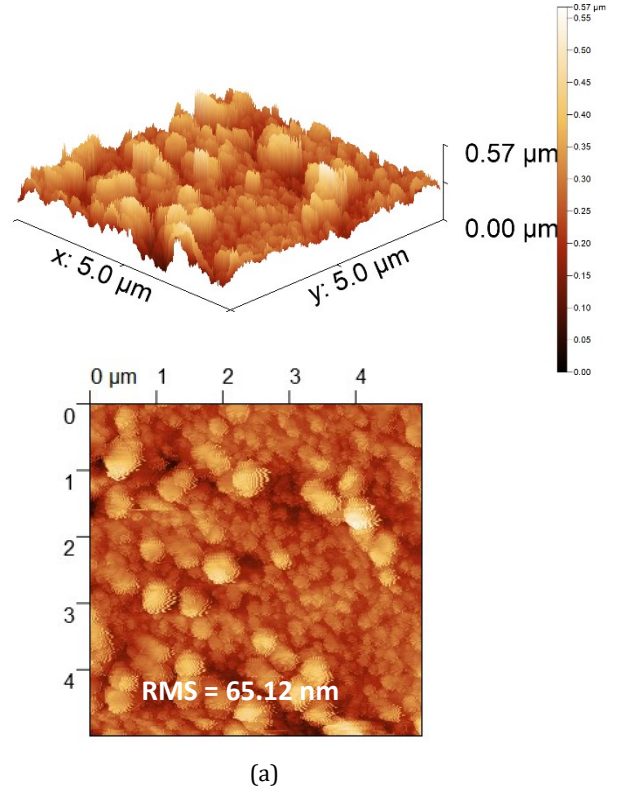


(a)



(b)

**Figure 4.** The provided images depict Atomic Force Microscopy (AFM) scans in both two-dimensional (2D) and three-dimensional (3D) views of ZnO thin films on an n-Si substrate. These films include both undoped and Ir-doped samples.
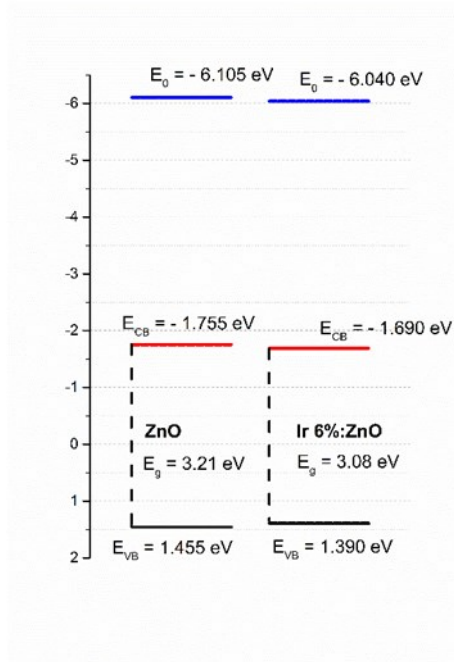
**Figure 5.** The positions of the conduction and valence band edges in the thin films of ZnO and ZnO doped with Ir

Figure 6 displays the experimental semi-logarithmic current-voltage (I-V) behaviors of the manufactured photodiodes. These measurements have been performed at room temperature under different light intensities and in the absence of light. The aim was to deduce the electrical characteristics of the diodes. The non-linear patterns observed can be elucidated through the application of the thermionic emission model, which is expressed by the following equation [24].

$$I = I_0 \left[ \left( exp \frac{qV}{nkT} \right) - 1 \right] \qquad (5)$$

Here, $I_0, q, n, k, T, and\ V$ represent the saturation current, elementary charge, ideality factor of the diode, Boltzmann constant (in Kelvin), and applied voltage, correspondingly.

$$I_0 = AA^* T^2 exp \left( - \frac{q\Phi_b}{kT} \right) \qquad (6)$$

In this equation, A represents the contact area of the diode (approximately $7.85 \times 10^{-3}$ cm$^2$), A* stands for the Richardson constant specific to ZnO (A* = 32 A/cm$^2$K$^2$), and $\Phi_b$ signifies the Schottky barrier height, which can be calculated using Equation (6). The values of n and $\Phi_b$ acquired from the I-V plot have been compiled in Table 1.

The expected *n* values for an ideal contact should ideally be unity. However, *n* values exceeding 1 indicate deviations from the expected ideal contact, offering insights into how the incorporation of Ir into
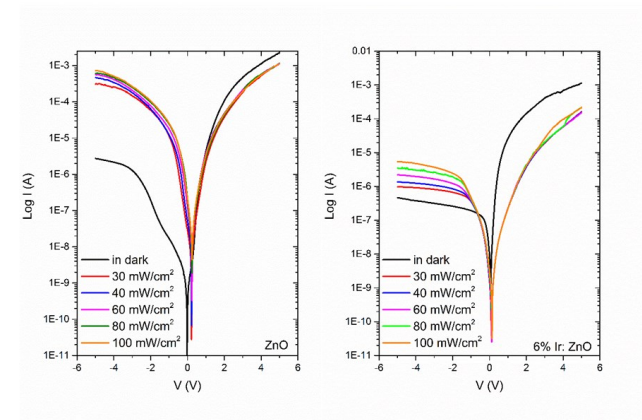


**Figure 6.** Current-voltage behaviors of the photodiodes in both absence of light (dark) and the presence of illumination.

ZnO affects diode performance. This effect is not solely ascribed to the degradation of surface conditions due to the inclusion of Ir, but also stems from diminished crystal quality, a factor that notably affects the excellence of the metal-semiconductor junction. Hence, the presence of consistent barrier height and the existence of interface states might help elucidate the occurrence of n surpassing unity, even without significant changes in barrier height. Table 1 emphasizes that the barrier height ($\Phi_b$), as derived via using the I-V characteristics, decrease as Ir is introduced into the photodiodes.

To ascertain the diode's series resistance and barrier height, the Norde method was employed, as defined by the subsequent equation [25],

$$F(V) = \frac{V_0}{\gamma} - \frac{kT}{q} \left( \frac{I(V)}{AA^* T^2} \right) \qquad (7)$$

Here, $\gamma$ is a number (unitless) larger than *n*. I(V) represents the current derived from the I-V characteristic. Figure 7 illustrates the graph depicting F(V) against voltage for the diode.

**Table 1**. The computed electrical and optoelectrical parameters of the fabricated photodiodes.

|  | *n* |  | $\Phi_B$ (eV) |  |  | $R_s$ (kΩ) |  |  |
|---|---|---|---|---|---|---|---|---|
|  | (I-V) | (dV/dlnI) | (I-V) | (Norde) | (H-I) | (Norde) | (dV/dlnI) | (H-I) |
| **ZnO** | 5.90 | 6.77 | 0.52 | 0.82 | 0.68 | 2.86 | 7.89 | 27.95 |
| **6% Ir: ZnO** | 4.48 | 6.18 | 0.47 | 0.81 | 0.45 | 4.29 | 7.90 | 27.86 |

Within the Norde method, the definition of the barrier height is as follows,

$$\Phi_B = F(V_0) + \frac{V_0}{\gamma} - \frac{kT}{q} \tag{8}$$

where $F(V_0)$ corresponds to the lowest value of $F(V)$. The determination of the series resistance ($R_s$) is based on the subsequent equation:

$$R_s = \frac{kT(\gamma - n)}{qI_1} \tag{9}$$

In this equation $\gamma$ is the integer (unitless) bigger than $n$, $q$ denotes an electron charge and $I_1$ shows the current acquired from the minimum point of $F(V)$. The $\Phi_B$ values of the photodiodes were determined as 0.81 eV and 0.82 eV for ZIRO0 and ZIRO6, respectively. The $R_s$ values of the photodiodes were calculated as 2.86 kΩ and 4.29 kΩ for ZIRO0 and ZIRO6, respectively. While $\Phi_B$ values calculated using this method almost did not change with the dopant, it was observed that the value of $R_s$ increased with the dopant.

In diodes, the presence of $R_s$ typically results from factors such as the resistances of top and bottom contacts, layer resistances, non-uniform interface states, and variations in barrier height.

This value is closely connected to the difference in work functions between Si (4.97 eV) and ZnO (4.25 eV), resulting in a gap of 0.72 eV.
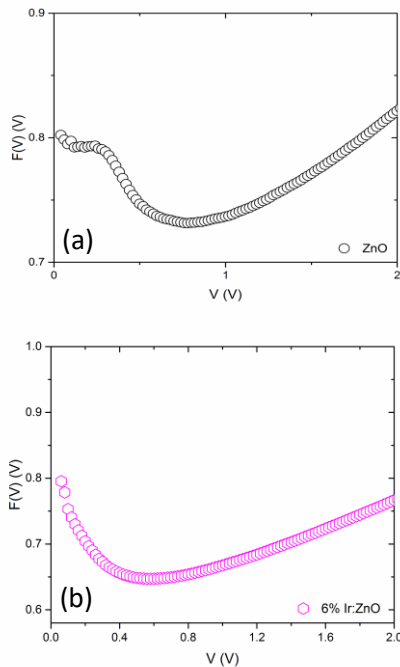


**Figure 7.** $F(V) – V$ plots of photodiodes

The value of $R_s$, crucial for metal-semiconductor contact assessment and a significant factor contributing to the departure from ideal diode behavior, has the potential to influence diode electrical performance. The approach to ascertain this involves employing Cheung's technique, specifically in the range of elevated current where the linear nature of the I-V characteristic deviates. This method, capable of deriving both $n$ and $\Phi_B$ values, characterizes the forward-biased I-V response of a component that includes series resistance, using the following equation:

$$I = I_0 exp\left(\frac{q(V - IR_s)}{nkT}\right) \tag{10}$$

The equations provided below is utilized to find the $n$, $R_s$ and $\Phi_B$ values,

$$\frac{dV}{d(lnI)} = IR_S + \frac{nkT}{q} \tag{11}$$

$$H(I) = n\Phi_B + IR_S \tag{12}$$

$$H(I) = V - \frac{nkT}{q} ln\left(\frac{I}{AA^*T^2}\right) \tag{13}$$

The plots depicting the forward-bias dV/d(lnI)-I characteristics of the heterojunction diodes are displayed in Figure 8. The intersection point furnishes the n value for these diodes. The computed n values are detailed in Table 1. The differences observed between the $n$ values derived from the forward-biased semi-log I-V plots and those obtained from the dV/d(lnI)-I plots can be attributed to undesired interface states and variations in the voltage ranges utilized in the calculations. Nonetheless, in both approaches, the $n$ value decreased with the introduction of Ir doping.

The graphs illustrating the relationship between $H(I)$ and $I$ are presented in Figure 8. The gradient of this plot provides the $R_s$ value, while the point of intersection yields the $\Phi_B$ value. The computed values are detailed in Table 1. The $\Phi_B$ values obtained with the standard TE theory, the Norde method and the $H(I) - I$ plot decreased with the Ir doping, but the calculated $\Phi_B$ values showed numerical differences with each other.

This distinction is commonly linked to the non-uniformity of the barrier and the less-than-ideal characteristics of the diodes.

The determined $R_s$ values derived from both the $R_s$ plots and the $H(I)$ function are notably elevated. The calculated $R_s$ values show slight discrepancies between the two calculation methods, possibly attributable to variations in barrier height uniformity [26,27]. The $R_s$ value of p-n heterojunction diodes is influenced by factors beyond the conductivity of the deposited thin films; it is also affected by contact resistance and the presence of the SiO₂ oxide layer

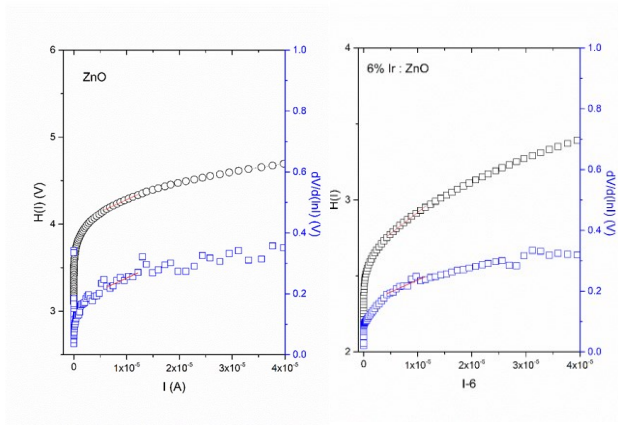[28]. Achieving a low $R_s$ value is crucial for attaining optimal performance in device applications.



**Figure 8.** The plots depict the forward bias $dV/d(lnI)$ - $I$ and $H(I)$ – $I$ relationships.

As evident from Table 1, a disparity exists between the $R_s$ and $\Phi_B$ values acquired through the Cheung and Norde methods. This divergence in outcomes can be attributed to the distinct applicability of both methods across various forward voltage ranges [29,30]. While Cheung's approach is confined to the nonlinear sector of forward bias, the Norde method extends across the complete forward bias segment of the $I–V$ plot. The increased $R_s$ (series resistance) values within the diodes can be ascribed to the nature of the rear ohmic contact and the layers formed from inorganic/organic materials on the silicon substrate [28,31]. Moreover, $R_s$ can be regarded as the Ohmic loss encompassing the entire device. As a result, the $R_s$ values of the diodes are impacted not only by the conductivity of ZnO films, but also by elements like electrodes, connections between metal and inorganic components, and unintended probe resistance [32].

As depicted in Figure 6, it is evident that all the manufactured photodiodes exhibit non-linear $I–V$ characteristics and rectifying behavior, as demonstrated by rectification ratio ( $RR = I_F/I_R$ ), (dark, ±5 V) values ranging from $10^2$ to $10^3$, as illustrated in Figure 9. Additionally, the I-V traits of the diodes are notably affected because of Ir doping. The highest RR value, amounting to $2.42 \times 10^3$ at ±5 V, was obtained from the ZIRO6 diode. The raised RR rectification ratio) values noted in the fabricated diodes can be explained by the augmented carrier concentration within the thin films. This can stem from the substitution of $Ir^{4+}$ ions at $Zn^{2+}$ lattice sites or the enhancement of the interface between the thin films and p-Si, as elaborated upon in references [33,34]. As observed in Figure 9, the RR values of the photodiodes exhibit a reduction with increasing illumination intensity, manifesting a non-linear pattern. It is interpreted that electrons within the valence band of the illuminated photodiodes traverse into the conduction band due to light absorption. This phenomenon signifies the manifestation of photoconductive characteristics in the photodiodes.

The subsequent equation was employed to investigate the photoconduction process of the heterojunction diodes [35];

$$I_{ph} = AP^\delta \quad (14)$$

In this context, $I_{ph}$ represents the photocurrent, while $A$ stands for a constant. The variables P and $\delta$ signify illumination intensity and illumination coefficient, respectively. The $\delta$ value is uncovered from the gradient of the log ($I_{ph}$) plotted against log (P), and it provides insights into the photocurrent mechanism of the device.
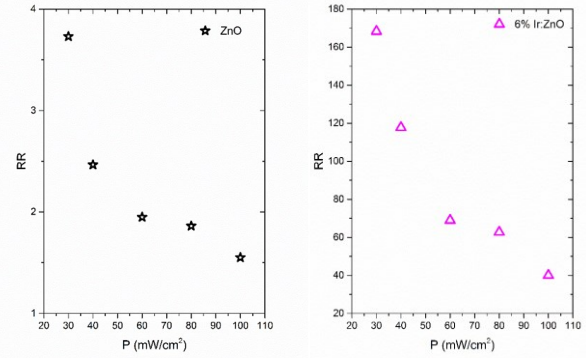


**Figure 9.** The rectification ratio undoped and Ir doped ZnO fabricated photodiodes under various light power concentrations.

The graph depicting the logarithm of $I_{ph}$ against the logarithm of P is presented in Figure 10. The $\delta$ values obtained were 0.633 for ZnO/p-Si and 1.407 for Ir:ZnO/p-Si heterojunction photodiodes. When $\delta$ equals 0.5 or 1, the photoconduction process in the diodes is associated with a bimolecular recombination process or a monomolecular recombination process, respectively. When the $\delta$ values fall within the interval of 0.5 to 1, the mechanism governing photoconductivity is associated with the presence of a continuous array of trapping sites within the band structure. Nevertheless, when the calculated $\delta$ value surpasses 1, the photoconductivity mechanism exhibits a behavior that is characterized by super linear tendencies, as elucidated in references [36,37,38].

The photoresponsivity (R), a pivotal parameter in photodiode characterization, can be computed using the subsequent equations:

$$R = \frac{I_p - I_d}{P \times A} \quad (15)$$

In this equation, $I_p$ stands for photocurrent, $I_d$ represents dark current, P signifies illumination power intensity, and A corresponds to the active area of the photodiode ($7.85 \times 10^{-3}$ $cm^2$). The obtained photoresponsivity values of photodiodes are illustrated in Figure 11. The photoresponsivity values

of the ZIRO6 tend to increase with increasing illumination intensity. The increased photoresponsivity is attributed to a substantial intrinsic barrier potential. This heightened intrinsic potential improves the transportation process and the dissociation of charges within the p-n heterojunction configuration [39,40].
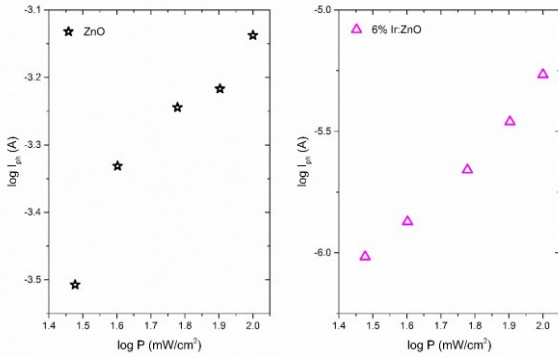


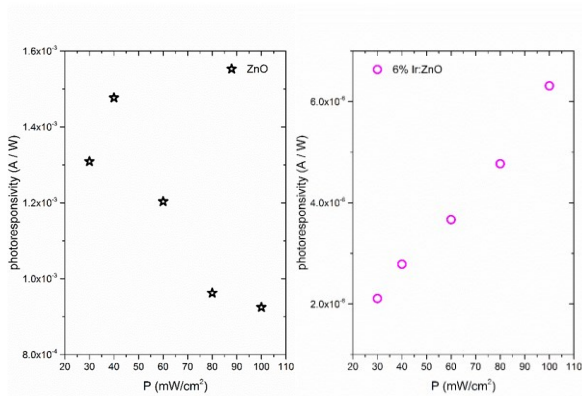**Figure 10.** The $m$ values were 0.633 (for ZnO) and 1.407 (for 6% Ir:ZnO).



**Figure 11.** The photoresponsivity of the manufactured photodiodes under varying light power levels.

Photosensitivity serves as a crucial parameter in the context of photosensor applications, quantified by the ratio of photocurrent to dark current ($I_{ph}/I_{dark}$). As depicted in Figure 12, the photosensitivity values of the photodiodes demonstrate an upward trend with rising illumination intensity. Notably, both manufactured photodiodes exhibit higher reverse currents when subjected to illumination compared to measurements taken in darkness. These findings collectively suggest that the photodiodes showcase photoconductive behavior.



**Figure 12.** Graphs illustrating the relationship between photosensitivity and illumination intensity of the diodes.
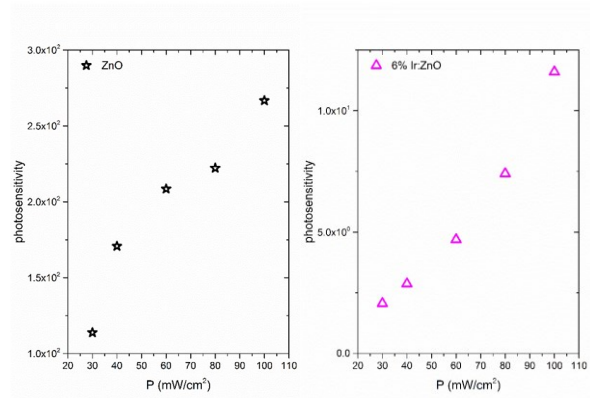
## 4. Discussion and Conclusion

Consequently, the sol-gel spin coating approach has been employed to fabricate heterojunction diodes comprising both ZIRO0 and ZIRO6. This study revealed the impact of Ir substitution on surface structures. Specifically, the surface roughness of ZnO, initially at 65.12 nm, demonstrated a reduction to 7.41 nm with a 6% Ir doping concentration. Furthermore, the introduction of Ir was found to induce a decrease in the $E_g$ of ZnO, shifting it from 3.21 eV to 3.08 eV. Electrical data obtained under various illumination intensities and dark conditions were utilized to analyze the optoelectronic properties of the photodiode. Notably, $n$ values exceeding 1 were observed, potentially attributed to the degradation of surface conditions and the compromised crystal quality resulting from Ir doping. Moreover, the barrier height ($\Phi_B$), as determined from $I-V$ characteristics, demonstrated a decrease in value upon Ir inclusion in the photodiodes. The calculated series resistance ($R_s$) values for ZIRO0 and ZIRO6 were 2.86 kΩ and 4.29 kΩ, respectively. Theoretical approaches, including the standard TE theory, the Norde method, and the $H(I)-I$ plot, yielded decreasing $\Phi_B$ values with Ir doping. However, numerical disparities among the calculated $\Phi_B$ values were observed, often attributed to barrier inhomogeneity and the non-ideal behavior of the diodes. Furthermore, Ir-doped ZnO photodiodes exhibited higher rectification ratios compared to their undoped counterparts. Interestingly, the photoresponsivity of fabricated Ir-doped photodiodes was noted to be lower than that of undoped ZnO photodiodes at varying light power levels. Additionally, the undoped ZnO photodiode showcased photosensitivity compared to the Ir-doped photodiode.

### Declaration of Ethical Code

## References

[1] Zhang, T., Li, M., Chen, J., Wang, Y., Miao, L., Lu, Y., He, Y., 2022. Materials Science & Engineering R 147 100661.

[2] Sharma, P., Hasan, M. R., Mehto, N. K., Deepak, Bishoyi, A., Narang, J., 2022. Sensors International 3, 100182.

[3] Atay, F., Gultepe, O., 2022. Applied Physics A 128:99.

[4] Agrohiya, S., Dahiya, S., Goyal, P. K., Rawal, I., Ohlan, A., Punia, R., and Maan, A. S., 2022. ECS Sensors Plus, 1 043601.

[5] Mahajan, L.M., 2023. Materials Today: Proceedings 73 464–467.

[6] Khan, A. R., Ramzan, M., Imran, M., Zubair, M., Shahab, S., Ahmed, S. J., Ferreira, F. and Iqbal, M. F., 2023. Coatings, 13(1), 34.

[7] Zubkins, M., Kalendarev, R., Gabrusenoks, J., Plaude, A., Zitolo, A., Anspoks, A., Pudzs, K., Vilnis, K., Azens, A., J. Purans, 2017. Thin Solid Films 636 694–701.

[8] Babajani, N., Jamshidi, S., 2019. Journal of Alloys and Compounds 782 533-544.

[9] Dhanalakshmi, M., Saravanakumar, K., Lakshmi Prabavathi, S., Muthuraj, V., 2020. Inorganic Chemistry Communications 111 107601.

[10] Dhyani, A. M., Nautiyal, A., Kumar, N., Rathi, S., Kumar, D., 2023. Materials Today: Proceedings 73 195–199.

[11] Joshi B. C., and Chaudhri, A. K., 2022. ACS Omega, 7, 21877–21881.

[12] Caglar, Y., Ilican, S., Caglar, M., Yakuphanoglu, F., 2010. J Sol-Gel Sci Technol 53:372–377.

[13] Yadav, A. B., Rawat, G., Sannakashappanavar, B. S., 2022. Materials Today Communications 31 103751.

[14] Sengun, P., Tumerkan Kesim, M., Caglar, M., Savaci, U., Turan, S., Sahin, İ., Suvaci, E., 2020. Powder Technology 374 214–222.

[15] Yakuphanoglu, F., Ilican, S., Caglar, M., Caglar, Y., 2010. Superlattices and Microstructures 47 732743.

[16] Elsheikh, N. Y., Battisha, I. K., Arais, A. A., Shams, M.S. 2022. Egypt. J. Chem. Vol. 65, No. SI:13B pp. 949 – 957.

[17] Ţalu, S., Boudour, S., Bouchama, I., Astinchap, B., Ghanbaripour, H., Saeed Akhtar, M., Zahra, S., 2022. Microsc Res Tech. 85:1213–1223.

[18] Zekry, A., 2019. Electronic Devices with Physical Insight, Ain Shams University, LAP LAMBERT Academic Publishing, May 16.

[19] Polat, O., Caglar, M., Coskun, F.M., Coskun, M., Caglar, Y., Turut, A., 2020. Vacuum 173, 109124.

[20] Polat, O., Coskun, F.M., Yildirim, Y. et al. 2023. Appl. Phys. A 129, 198.

[21] Kubelka, P., Munk, F., 1931. A contribution to the optics of pigments. Z. Technol. Phys. 12, 593–599.

[22] Chi, P.W., Wei, D.H., Wu, S.H., Chen, Y.Y., Yao, Y.D., 2015. RSC Adv., 5 pp. 96705-96713.

[23] Chao, C.H., Chi, P.W., Wei, D.H., 2016. J. Phys. Chem. C, 120, pp. 8210-8219.

[24] Sze, S.M., 1981. Physics of Semiconductor Devices. 3rd. WILEY. 578s.

[25] Norde, H., 1979. J. Appl. Phys. 50 5052.

[26] Li, Y., Li, Y., Zhang, J., Tong, T., Ye, W., 2018. J. Phys. D. Appl. Phys. 51, 095104.

[27] Polat, O., Coskun, M., Efeoglu, H., Caglar, M., Coskun, F.M., Caglar, Y., Turut, A., 2021. J. Phys. Condens. Matter 33, 035704.

[28] Ilican, S., Caglar, M., Aksoy, S., Caglar, Y., 2016. J. Nanomater. 2016, 6729032.

[29] Karatas¸, S., Yildirim, N., Türüt, A., 2013. Superlattice. Microst. 64 483–494.

[30] Aksoy Pehlivanoglu, S., 2021. Physica B: Condensed Matter Volume 603, 15 February, 412482.

[31] Giri, P., Chakrabarti, P., 2016. Superlattice. Microst. 93 248–260.

[32] Ko, C.J., Lin, Y.K., Chen, F.C., Chu, C.W., 2007. Appl. Phys. Lett. 90, 063509.

[33] Xu, X., Shukla, S., Liu, Y., Yue, B., Bullock, J., Su, L., Li, Y., Javey, A., Fang, X., Ager, J.W., 2018. Phys. Status Solidi Rapid Res. Lett. 12 1700381.

[34] Postica, V., Hoppe, M., Gr€ottrup, J., Hayes, P., Robisch, V., Smazna, D., Adelung, R., Viana, B., Aschehoug, P., Pauporte, T., Lupan, O., 2017. Solid State Sci. 71 75–86.

[35] Bube, R.H., 1960. Photoconductivity of Solids, Wiley, New York.

[36] Khusayfan, N.M., 2016. J. Alloys Compd. 666 501–506.

[37] Mekki, A., Dere, A., Mensah-Darkwa, K., Al-Ghamdi, A., Gupta, R.K., Harrabi, K., Farooq, W. A., El-Tantawy, F., Yakuphanoglu, F., 2016. Synth. Met. 217 43–56.

[38] Kazim, S., Ali, V., Zulfequar, M., Mazharul Haq, M., Husain, M., 2007. Phys. B Condens. Matter 393 310–315.

[39] Amiruddin, R., Santhosh Kumar, M.C., 2017. Nanosci. Nanotechnol. Lett. 9 489–495.

[40] Tan, L., Curtis, M.D., Francis, A.H., 2003. Chem. Mater. 15 2272–2279